Multi-Objective Optimization of Residual Stress and Cost in Laser Shock Peening Process Using Finite Element Analysis and PSO Algorithm

Sa'id Golabi, Mohammad Reza Vakil & Behzad Amirsalari

Lasers in Manufacturing and Materials Processing

ISSN 2196-7229

Lasers Manuf. Mater. Process.
DOI 10.1007/s40516-019-00102-1

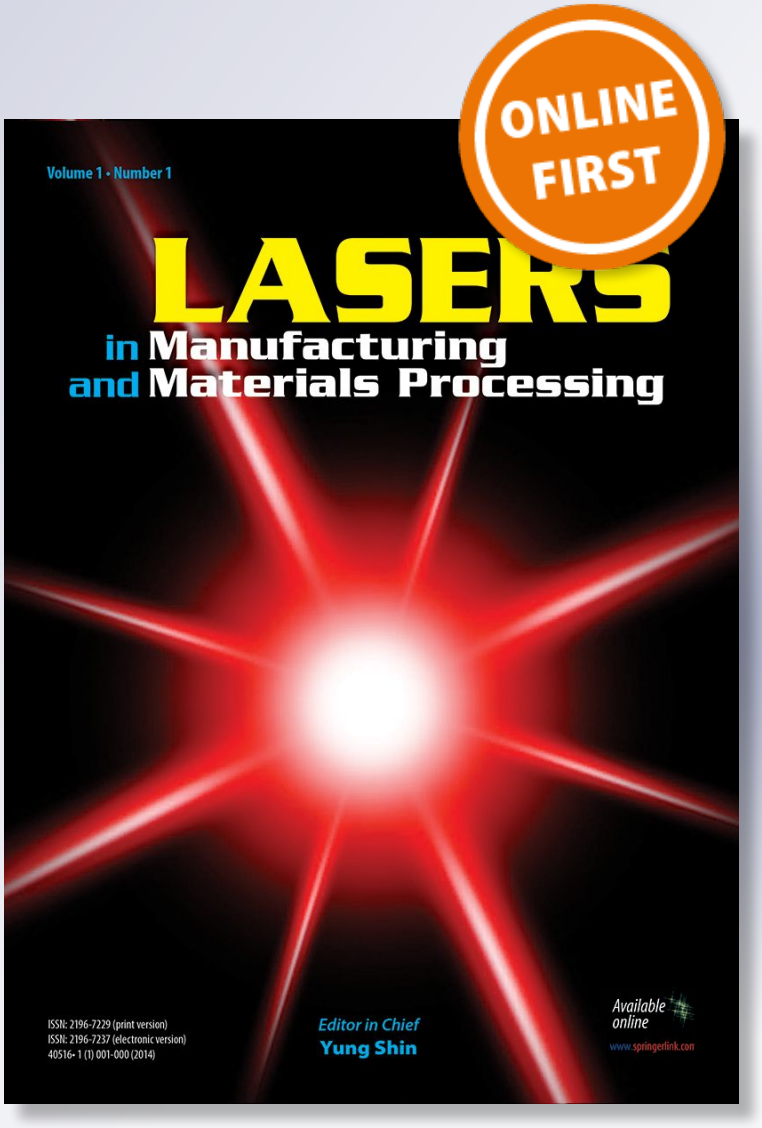

Springer

Lasers in Manufacturing and Materials Processing
https://doi.org/10.1007/s40516-019-00102-1

Multi-Objective Optimization of Residual Stress and Cost in Laser Shock Peening Process Using Finite Element Analysis and PSO Algorithm

Sa'id Golabi[1] · Mohammad Reza Vakil[1] · Behzad Amirsalari[1]

Accepted: 19 August 2019/Published online: 13 September 2019

Abstract

Laser shock peening (LSP) is an effective process utilized for surface enhancement of metal parts so that generating compressive residual stresses (RS) on the surface improves fatigue life of the material. The main affecting parameters on surface negative residual stress are laser power, laser beam size and shape, peening pitch and pattern. Varying these parameters alters the magnitude and depth of RS as well as the cost of LSP. An integrated method for simulation of optimum LSP process is presented in this paper, in which Particle Swarm Optimization (PSO) technique was employed utilizing Python coding in ABAQUS finite element environment to maximize the uniformity of compressive RS and minimize LSP cost on an Inconel 718 super-alloy specimen. The mentioned affecting parameters were selected as optimization parameters, and minimum acceptable amounts and depth of compressive RSs were two main design constraints. Simulation results were compared with previously published experimental ones, and optimum LSP variables were finally determined and presented for certain amount of design constraints. It was revealed that, relatively small circular laser beam, shot by square scanning pattern, leads to generate the most uniform RS with minimum LSP cost.

Keywords Laser shock peening · Residual stress · Particle swarm multi-objective optimization · Python coding · Finite element simulation

Introduction

Laser Shock Peening (LSP) is a surface operation that improves the mechanical properties and performance of metal parts. By laser peening, the residual

✉ Sa'id Golabi
golabi-s@kashanu.ac.ir

[1] Faculty of Mechanical Engineering, University of Kashan, Kashan, Iran

compressive stress on the surface of a sample increases, and therefore the strength and fatigue life enhance [1]. LSP operation is commonly used to increase properties such as fatigue life, corrosion resistance, tensile strength and hardness of metals [2–4]. The LSP process can be used for a wide range of metals, including cast iron, aluminum alloys, titanium alloys, nickel based super alloys, and other useful metals in industry for various applications including: turbine blades, rotor components, discs, shafts, gears, and bearing parts [5, 6].

Fabro et al. [7] developed a model to analytically describe three different steps for LSP process. In the first step, a high-pressure plasma was produced during the laser impact time. The second step includes adiabatic cooling of this plasma while the laser beam was shut down, and the third step was adiabatic cooling of recombined plasma during the previous step, which was not strong enough to create a plastic deformation. They showed that the impulse momentum was mostly generated in the final step, and could validate their model experimentally for confined geometries. Meanwhile, there were several parameters affecting the residual stresses resulted by LSP process. Here, it should be considered that confining the target material by a transparent layer plays a vital role in the pressure might and duration. Water confinement regime (WCR) was one of the most effective regimes to enhance the laser pulse pressure in comparison with the time when direct regime configurations were used. Hence, Wu and Shin investigated this regime and presented a self-closed thermal model [8] accompanied with self-closed one- and two-dimensional hydrodynamic models [9, 10] to simulate the LSP process regarding laser-matter interactions and responses of the material vicinal to the water coating interface. These models have no free variables demanding experimental evaluations under the same conditions. Their studies led to present and validate experimentally a comprehensive self-closed model [11] to simulate residual stresses generated in the substrate material by LSP in which three submodels including breakdown-plasma, confined-plasma, finite element mechanics models, were sequentially applied. Furthermore, to decode the effect of interactions between laser and coating material on residual stresses induced on the target material, they cooperated with Cao to publish a study [12] in which three states of LSP process including single shot, single-track, and multi-track overlapping, for 4140 steel parts coated with black paint were investigated via finite element analysis and experimental measurements. They investigated the effect of process parameters on generated residual stresses and compared the predicted indentation profiles with experimented ones proving the accuracy of their work.

In order to improve the laser shock peening process, several experimental studies have been conducted to investigate the effect of laser shock peening parameters. However, due to the complexity of the dynamic response of materials subjected to this process, it is difficult to monitor the process by existing tools. Therefore, in order to overcome such problems and predict material behavior in LSP process, simulation can be an effective solution. Hence, Wei et al. [13] presented a complete three-dimensional finite and infinite element model to predict residual stresses regarding their formation,

value, and distribution due to LSP process. They presented a parametric investigation and validated this model by comparing its results for a specific case with experimental ones, and afterwards, they analyzed influence of various involved parameters in their study. Keller et al. [14] numerically and experimentally investigated the effect of laser power density and laser beam area on the RS generated by LSP process on AA2198 aluminum alloy. They showed that, smaller laser beam area leads to higher value of compressive stresses, with lower penetration depth. Ji-Soo-Kim et al. [15] also studied the effect of LSP process on RS of an Alloy-600 sample using numerical methods. Utilizing Johnson-Cook model, they compared their results with previously published papers. Based on their study, LSP process is more effective on samples with higher tensile residual stress, nevertheless, the effective depth decreases with increase in initial tensile RS and initial strain. Warren et al. [16] worked on simulation, analysis and validation of laser shock peening process. They examined the effect of laser intensity, laser beam diameter, and laser pulses overlap on RSs and strains. They showed that enhancement of laser intensity increases the value and depth of compressive residual stresses and validated their results with other researches.

Moreover, using small-diameter laser beam leads to reduction in effective depth of compressive residual stress. Shuai Huang et al. [17] have experimentally investigated the effect of laser shock peening processes with different powers on impact toughness and the affects generated in metal microstructure. According to their results, impact toughness depends on the laser beam energy and increases from about 2% to a maximum value of 64% comparing with the samples not laser shock peened. Wu et al. [18] performed a numerical simulation of the LSP process using femtosecond lasers and compared their results with experimental data. They showed that femtosecond laser increases the value of RS near the surface but decreases its penetration depth. The results of this process also varies with other parameters. Xu et al. [19] investigated the effects of two different scanning paths and three overlapping rates, i.e. 30%, 50% and 70%, on RS distribution over a 316 L stainless steel blade by LSP process, in which only square beam shape with constant size was used. Sathyajith et al. [20] examined the effect of laser shock peening process on the hardened aluminum alloy 6061 using low-energy laser. They measured the value and depth of generated RS on the surface. Additionally, the size of the crystals and micro-strains on the surface were obtained and compared with the data acquired before laser shock peening process. An increase of 190% in value of compressive RS on the surface as well as 1.2 mm RS depth were their most important achievements.

One of the main frequent objectives of recent publications in this area, is reaching the highest possible compressive residual stress. Accordingly, Prabhakaran et al. [21] determined the optimum state of LSP process for austenitic stainless steel by adjusting pulse density and overlap percentage. While, Singh [22] considered pressure pulse duration, magnitude of the pressure pulse, size and shape of laser effective point, thickness of the samples, overlap size and peening sequence as variables in his simulation and optimization study.

He used particle swarm algorithm for optimization in order to improve material fatigue and corrosion properties. Chupakhin et al. [23] studied the effects of some LSP input parameters such as laser pulse energy, number of treatment overlaps and laser spot size on the final RS distribution, characterized by three different quantities. They practically experienced all possible scenarios using full factorial design of experiments, and enhanced fatigue life of the specimens. Moreover, Sibalija et al. [24] modeled and optimized the LSP process considering an integrated simulated annealing algorithm. In order to determine the optimal process parameters during a test, they considered different values for voltage, focus position and pulse duration parameters. They also showed that the surface of the material after optimization process is smoother than before, and the average roughness will be much less than that before optimization. In addition to surface properties, their optimization led to favorable microstructural changes and hardening. Amarchintaa et al. [25] used reverse optimization of material models to simulate RSs caused by LSP process. They used FE method to predict the RSs resulted due to LSP process. They also compared the results of their simulations with other experimental results. They utilized three material models of Johnson-Cook, Zerilli-Armstrong and Khan-Huang-Liang to simulate material behavior. They plotted the performance of each model and obtained the results of various test models, and observed a slight difference between their simulation and experimental results. Zhao et al. [26] simulated the RSs induced by LSP process using FE method and investigated its effects on crack propagation. They introduced the best scanning pattern for the process with a crack reduction approach. M. Frija et al. [27] simulated LSP process using FE method and optimized its parameters using Response Surface Method (RSM) in Design of Experiments (DoE) technique. In their other paper [28], in order to predict and optimize LSP process, an artificial Neural Network in MATLAB software was employed and trained by FE results. Hence, they could numerically model the process and predict the results of other combination of LSP variables. However, it is obvious that the prediction is not as much accurate as writing the optimization code inside a FE environment. Bhamare et al. [29] simulated and optimized LSP process parameters to improve the lifetime of the flexural fatigue of Ti-6Al-2Sn-4Zr-2Mo alloys. They considered RS as a function of laser parameters (energy, laser pulse width and spot diameter, geometry, materials and sequences of laser shots. Additionally, using a numerical method based on the nonlinear three-dimensional FE method, they examined the relationship between the process parameters and the distribution of residual stress. Moreover, they showed the effect of laser parameters and sequences of laser strokes on the final RS distribution in their simulation. They used the Zerilli-Armstrong model to display the response of the materials at a high strain rate in LSP process. The results of their research were compared with experimental results, and showed that choosing an optimal set of parameters can lead to a significant increase of flexural fatigue life. Moreover, Kumar et al. [30] presented a method for optimizing the parameters of LSP process using Taguchi algorithm. In their research, optimal values for overlapping laser pulses, duration of each pulse, and density of energy pulses were obtained to achieve optimal RS state and distortion.

Since most cracks are generated during high local tensile stresses during dynamic loading, various methods are implemented to generate a compressive residual stress at locations where fatigue crack initiates and starts to grow, including shot peening and laser shock peening processes. Despite shot peening, a proper LSP process does not make any bad effect on the quality of peened surface. Nevertheless, improper generation of residual stresses may itself lead to generation of not only stress concentration points but also a surface with irregular amounts of compressive residual stresses. Thus, cracks tend to initiate and grow from the locations with less compressive residual stresses. Besides, generation of a regular peened surface need a planned LSP process to cover the whole proposed surface and meanwhile avoid extra peening which leads to extra cost. Thus, the necessity for considering the cost of peening forces to determine the most suitable distance between the shots and is also a tradeoff between power and other laser peening parameters. Finally, the amount and depth of compressive RS are other important issues that vastly depends on LSP parameters. Thus, two main important objectives considered simultaneously during this research are the uniformity of RS on the surface of target part as well as the cost of process, which could be derived from LSP parameters and FE results respectively, to eventually form a multi-objective function. The optimum LSP variables are needed to be determined so that these two objectives could be achieved at the same time. Meanwhile, Inconel 718 super-alloy has a vast range of applications in rotary machines, such as turbine blades, which are highly exposed to flow of hot combustion gases, making them to face high risk of corrosion, pitting and fatigue failure. Hence, the optimum LSP parameters are investigated through a straightforward method in order to achieve the highest uniformity of compressive RS and minimum peening cost for an Inconel 718 super-alloy specimen. Obviously, the experimental research on laser shock peened parts are difficult and expensive, thus ABAQUS software is employed to simulate the process. Moreover, in order to investigate multi-objective optimization, PSO code is written using Python programming language inside ABAQUS environment and each time new models were created using the new proposed population generated by PSO. The result of each analysis were then used for generation of new population till the termination conditions are satisfied. During optimization, minimum acceptable amounts and penetration depth of RSs on the surface were considered as design constraints. Finally, the optimum LSP parameters leading to the best desired results, including the optimized input power, shape and size of the laser beam, and scan pitch and pattern were researched in this paper.

Laser Shock Peening Process

During laser peening process a high-energy laser pulse concentrates on a metal surface, passes through a transparent layer and reaches the opaque layer on the surface and heats it locally. The heated region on the surface

evaporates and reaches a temperature of more than 10,000 °C and changes the phase of generated gas to plasma due to ionization [7, 31]. Plasma explosion with high temperature on the surface leads to a high pressure pulse on the surface and consequently propagates a shock wave inside the object as shown in Fig. 1 [27, 32].

Fabro et al. [7] presented a model for calculating plasma pressure that is the main affecting parameter on RS in LSP process. Based on this model, the physical model for predicting pulse pressure as a function of laser power density is determined by Eq. 1 and shown in Fig. 2 [7].

$$\begin{aligned} I(\mathrm{t}) &= \mathrm{p}(\mathrm{t})\frac{dL(\mathrm{t})}{dt} + \frac{3}{2a}\frac{d}{dt}[\mathrm{p}(\mathrm{t})L(\mathrm{t})] \\ V(\mathrm{t}) &= \frac{dL(\mathrm{t})}{dt} = \left[\frac{1}{Z_1} + \frac{1}{Z_2}\right]\mathrm{p}(\mathrm{t}) \end{aligned} \tag{1}$$

In Eq. 1, I and V represent density of the laser power and plasma expansion pace during laser radiation respectively, P stands for pulse pressure, and L is the thickness of plasma as a functions of time (t). Here, α is the efficiency of laser impact on surface, and the impact impedance (Zi) is obtained by:

$$Z_i = \rho_i D_i \tag{2}$$

In which ρ_i and D_i are material density and impact velocity, respectively. The index i identifies layer number of materials. When the laser power density is constant (I_0), the scale rule for pressure pulse can be estimated in accordance with Eq. 3 [7].

$$\mathrm{P(GPa)} = 0.01\sqrt{\frac{\alpha}{2\alpha+3}}\sqrt{Z\left(\frac{g}{cm^2 s}\right)}\sqrt{I_0\left(\frac{GW}{cm^2}\right)} \tag{3}$$

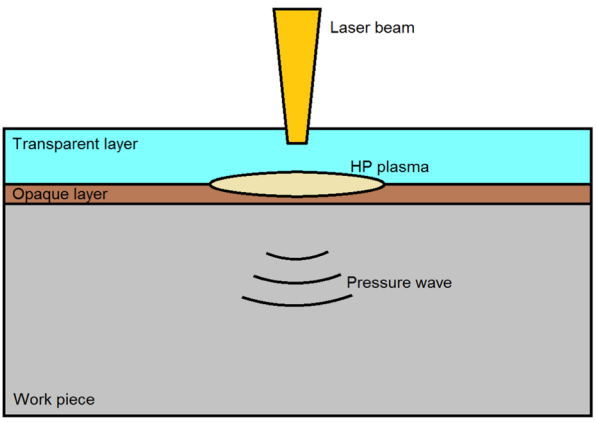

Fig. 1 General schematic of LSP process [27, 32]

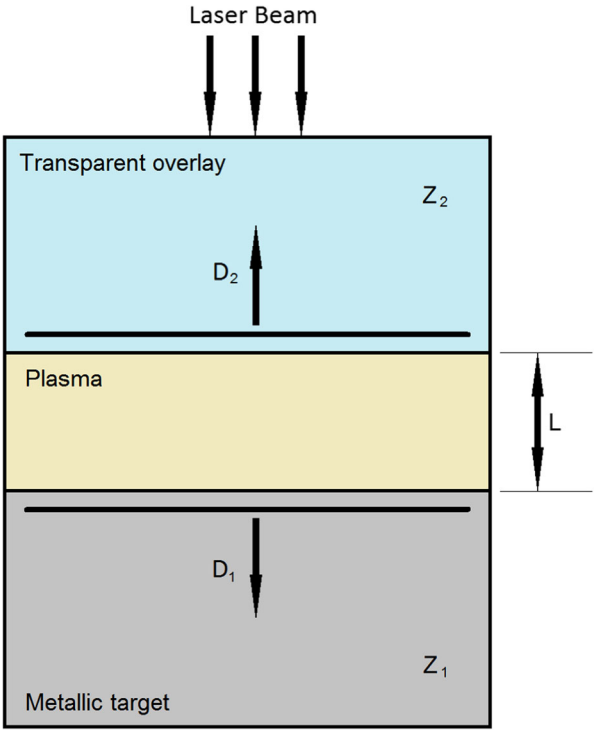

Fig. 2 Laser impact configuration [7]

In which P is peak pressure. During the period of impact, total energy E_T from the laser source is divided into two parts. The first part, αE, contributes in formation of a pressure pulse, and the next, *(1-α)E*, is spent on the production and ionization of the plasma. α is mostly between 0.2 to 0.5. Thus, Z, the impedance of combined impact, is defined by Eq. 4, in which, Z_1 and Z_2 are the impedances of base material and confining layer, respectively [7].

$$\frac{2}{Z} = \frac{1}{Z_1} + \frac{1}{Z_2} \tag{4}$$

Equation 3 shows that the pressure pulse strongly depends on the laser power density and impedance characteristic of the mid-space around the interference region. Here, if water is used as a confining layer in the process, Eq. 3 would be simplified to Eq. 5 [33].

$$P(\mathrm{GPa}) = 1.02\sqrt{I_0\left(\frac{GW}{cm^2}\right)} \tag{5}$$

The high plasma pressure, resulting from the collision of high energy laser pulse with the surface of material, usually has a Gaussian time profile with a maximum width of 50-60 ns [34]. The peak pressure depends on initial parameters of LSP process, and its value can be estimated from Eq. 5, when using water as a transparent layer. Peak

pressure is proportional to the root square of laser power density [33, 35], therefore, in FE simulation, laser power directly affects pressure on the surface, and its enhancement within a certain range increases the compressive RS [16].

In order to create and send a shock wave inside an object, the laser used for the process must be a pulse type. Shortening the pulse time increases the penetration depth of residual stresses, but reduces their values. The history of pressure-time is also very important for simulating LSP process. Although pressure-time history is usually defined as Gaussian time distribution, due to the very low width of the pulse, shape of the pulse pressure is very close to a triangular profile [36]. Thus, the pressure-time history for a single collision or multiple collisions can be simplified to a triangular distribution in which the pressure is raised linearly up to the peak and then reduces down to zero.

Considering the power of laser and the coefficient of material used for peening in Eq. 5, the peak pressure of a pressure pulse can be obtained and applied in simulation using a proper linear amplitude to create a triangular profile for each pulse. In Fig. 3, a compression is illustrated between Gaussian and simplified model with a peak value of 2.8 GPa and Full Width at Half Maximum (FWHM) of 50 ns.

Other laser parameters that affect simulation results are shape and size of a laser beam. The area of laser effect point along with laser power density generate laser pulse power. Moreover, the available laser effect points include circular, square and oval shapes. However, circular shape is the most commonly used shape in references. Other important parameter in simulation results, is the laser scan pattern. In this study, square and triangular scan patterns were considered. The laser shocks are juxtaposed in rows and in a "square" scan pattern (Fig. 4-a). Peening of every new row starts after peening the last row and just above it, in which the distance between every two row is equal to Y pitch while the distance between every two spot in a row is the X pitch. While, in the "triangular" scan pattern (Fig. 4-b) considering the X and Y pitch, the location of the first spot for the new row is in the middle of the former two spots in previous row.

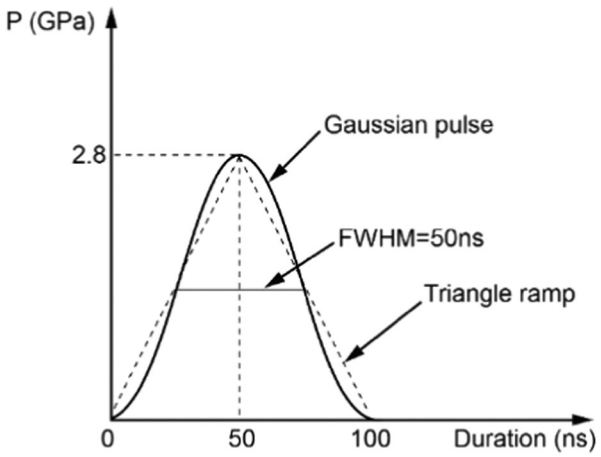

Fig. 3 Pressure-time history for one pals on the surface [32]

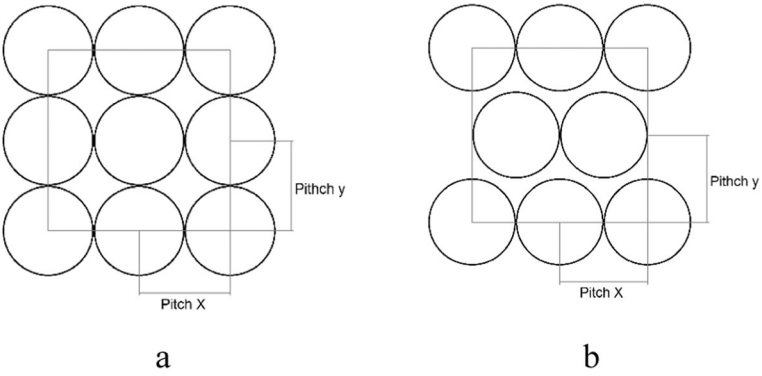

Fig. 4 Scan patterns (**a**) Square. **b** Triangular

Simulation Method and Validation

In order to simulate the process and determine short-time (dynamic stresses) as well as steady state responses (residual stresses) of impact, ABAQUS FE software has been implemented. Due to short duration of applying pulse pressure on the surface of sample, a complex impact wave produced on the surface of the material, goes through the model. This high-pressure wave generates dynamic stresses and causes plastic deformation in the regions where these stresses are more than the yield stress of part. Therefore, the first stage of simulation process is a dynamic stage in which effect of the impact caused by the pressure pulse must be checked, and then in the next step, the result of interaction between two elastic and plastic areas must be specified to acquire residual stresses.

There are two different types of solvers for solving problems in ABAQUS FE software: an implicit solver, and an explicit one. The ABAQUS explicit code can be used for dynamic response model to analyze the effect of plasma pressure pulse on the surface and calculation of dynamic stresses. Nevertheless, using this solver for the second stage leads to an enormous increase in calculation time, similar to using implicit solver for obtaining dynamic responses. Therefore, a combination of both types of solvers is the most efficient plan for solving this type of simulation problems, i.e., using the explicit solver in the first step to obtain the dynamic response and, employing the implicit solver in the second step, in which the static equilibrium must be happened. To use this method, the model must be initially created in the software and exposed to a pressure pulse and analyzed using explicit solver until the dynamic stresses are stabilized and the shock wave penetrates deep into the sample. The static equilibrium step will then start with the deformed object and all its stress and strain history, to obtain the RSs. The flowchart of the LSP simulation process is illustrated in Fig. 5.

After the stress wave penetrates into the sample, it gradually weakens and the value of the resultant stress decreases. During simulation of relatively thin parts, part of the shock wave reflects back when it reaches the boundary of the sample. In reality, this reflection occurs when the boundaries are rigid enough to return the wave. Since the reflected wave has very little energy, it can be neglected without losing the accuracy of

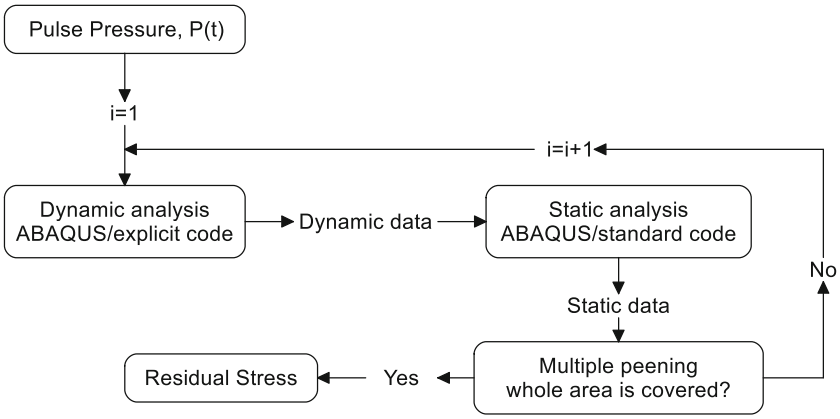

Fig. 5 Flowchart of the LSP simulation [32]

the analysis, and normally the stress wave continues to move and enter the next layer of material or environment. Therefore, in order to save time and amend the modeling approach, researchers used infinite elements around the model [32]. Two types of finite and infinite elements are used to mesh the model as shown in Fig. 6.

FE analysis can be used to calculate and show large nonlinear deformations and consequently can be utilized to find the effect of high impact pressure. On the other hand as explained above, the reflection of impact wave is not required to be considered in the analysis, therefore, around the finite elements of the model, infinite elements were used as non-reflective boundaries. These boundaries make the reflection of the stress wave to be minimized. The infinite elements were used in a region where the resulted stresses from LSP, did not exceed the elastic limit and LSP created no RSs in

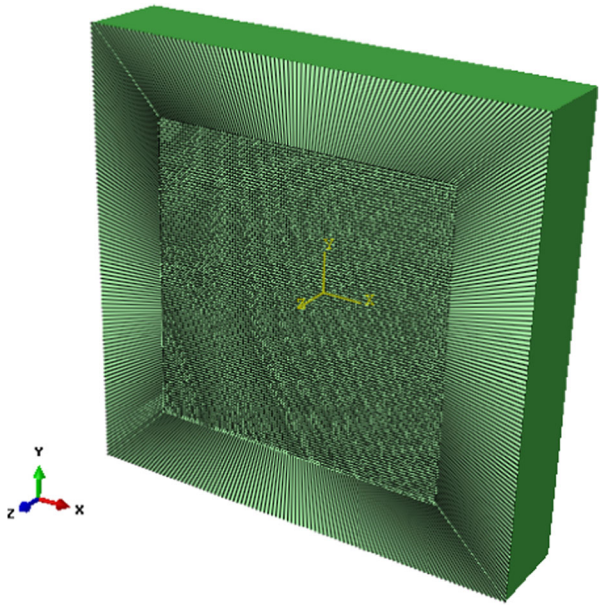

Fig. 6 Finite and infinite elements on part

that region. The utilization of infinite elements could also help to omit the reflection of shock waves in far areas from the impact point where LSP did not have any effect on RSs, and finally leaded to sharp decrease in calculation time. It must be noted that within dynamic step of analysis, infinite elements keep static stresses constant on the boundaries without any effect on stiffness, which leads to the generation of some rigid small body motion of the modeled region. These distortions are followed by some slight reactional RS in the static mode which due to considerable distance between boundaries and impact zone, do not interfere with generated LSP RS. Hence, the finite element region was increased when LSP RSs penetrate into the infinite region.

Before starting optimization process, the perfection of finite element simulation must be ensured and validated by other references. Accordingly, the model chosen by Ballard et al. [37] was proposed for justification. In their research, the impact of a square laser pulse to the center of a cube upper surface was investigated experimentally. That model has been simulated by different researchers including Ding and Ye [32]. The simulation methodology proposed in this research showed very good compliance with the results published by Ding and Ye [32].

In this research, a $10 \times 10 \times 5$ mm cubic piece of 35CD4 alloy steel with 50 *Rockwell C* hardness was modeled and subjected to a 5×5 mm square laser beam in the center of the upper surface. Since the laser beam impacts exactly at the center of the upper surface of the cube and in order to reduce the computational time, only one quarter of the cube was modeled. To simulate material behaviour through the LSP process, material model used for both validation and present study, is considered to be homogeneous isentropic and elastic-perfectly plastic. The central and marginal regions of model were meshed by eight-node brick elements with reduced integrations type C3D8R, and 8-node linear one-way infinite elements type CIN3D8, respectively. In order to reach reliable and comparable results for validation, the elements' size was converged to 0.0625 *mm* used by one of the references [32]. The proposed geometry and its material characteristics are depicted in Fig. 7 and Table 1 respectively.

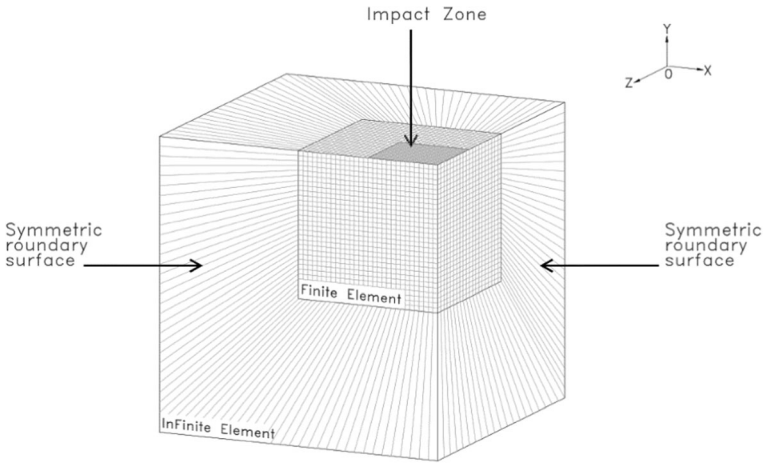

Fig. 7 Simulated quarter of model [32]

Table 1 Mechanical properties of Inconel 35CD4 with 50 Rockwell C hardness [32]

Mechanical property	Value
Mass density (Kg/m3)	7800
poisson's ratio	0.29
elasticity modulus (GPa)	210
dynamic yield stress (GPa)	1.24

This model was designed based on a test carried out by a Gaussian pulse type Q-switched Nd-glass laser with a power density of 8 GW/cm^2. A square laser pulse with Gaussian time distribution, peak pressure of 3GPa and 50 ns FWHM[1] was shot the 5 mm side.

The compressive RS was generated as the result of laser shock peening process, and the distribution of stress along Z axis of coordinates were determined and shown in Fig. 8. To investigate the accuracy of simulation, the data presented by Ding and Ye [32] diagrams were extracted using plot-digitizer software and compared. The dynamic RSs were initially evaluated 400 ns after the impact, and they were then determined long time after the impact.

In Fig. 9, the normal stress values on XY plane on the upper surface and the stress distribution in depth of sample after 4000 ns were presented. These figures show that the results obtained from the simulation in dynamic state were in good compliance with Ding and Ye's [32]. Figure 9-a indicates that the greatest value of stress occurs at the center point of the laser beam on the model surface and Fig. 9-b shows that the highest stress occurs on the surface and the absolute value of stress gradually decreases to zero in a depth of about 8.0 mm. The results of this research's dynamic stresses had also very good compliance with Ding and Ye's [32] results, thus it can be concluded that the proposed method for simulating the dynamic step is correct and reliable.

In order to obtain the distribution of RSs from dynamic stresses, a static analysis was performed and the results were compared with Ding and Ye's [32] and Ballard et al. [37]. Figure 10-a shows very good compliances between this study and the results presented in the above references for variation of stresses on the surface along the Z axis. According to this figure, the least amount of stress on the surface is about -360 MPa, and its absolute value decreases to zero along the Z axis after about 2 mm distance from the impact zone. Figure 10-b compares the stress variation along the depth of the part. As shown in this figure, the RS begins with −320 MPa value, and at about 0.6 to 0.7 mm in depth converges to zero. This depth is called the RS penetration depth. Figure 10. shows that the simulation results performed in steady-state have very good compliance with Ding and Ye's [32] simulation, and Ballard et al.'s experimental results [37]; and the method described for RSs simulation is also reliable.

A closer look at above figures reveals the differences between dynamic and static results. In Fig. 11-a and b, von Mises and normal dynamic stresses are shown respectively, telling that the stress on the surface is less uniform in contrary to Fig. 11-c and d with smoother stresses in static analyses. This can be attributed to the equilibrium of all elements in steady state.

[1] Full Width at Half-Maximum

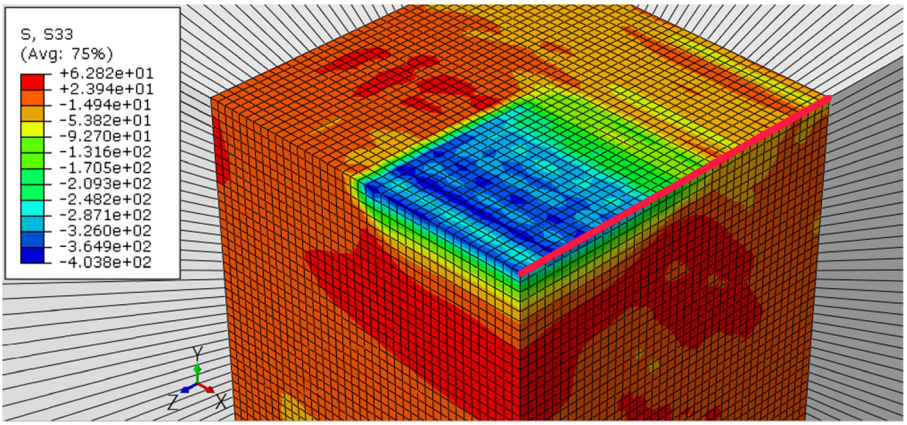

Fig. 8 Measurement path along Z axis

Simulation and Analysis

In this step, a 20 × 20 mm Inconel 718 super alloy with 3 mm thickness and 10 × 10 mm target area on the center of its upper surface is considered for LSP process, as shown in the hatched region of Fig. 12. In this target area, the constraints of optimization problem described later, including uniformity and RSs minimum value and depth, are investigated. Although accuracy of the results on surface is lower than that in depth, and the most destructive cracks are those started from the surface, researchers are motivated to investigate compressive RS as a way to reduce crack initiation on the surface. On the other hand, phase changes or any variation of metal grain size are not currently included in finite element softwares used for stress analysis and therefore are neglected in this research as well. Inconel 718 is a creep resistant material and widely used in rotary components construction, and its physical properties were given in Table 2. Moreover, a 5GW laser power with laser pulse duration of 100 ns with water as confining material were considered for this simulation.

Afterwards, the part was modeled with previously mentioned material model and mesh types, while it size still needs to be converged for this FE analysis. Although denser meshes might provide a more accurate results, they lead to more computational time and cost. Accordingly, by halving element dimensions, computation cost will increase by 16 times for a coupled analysis, therefore,

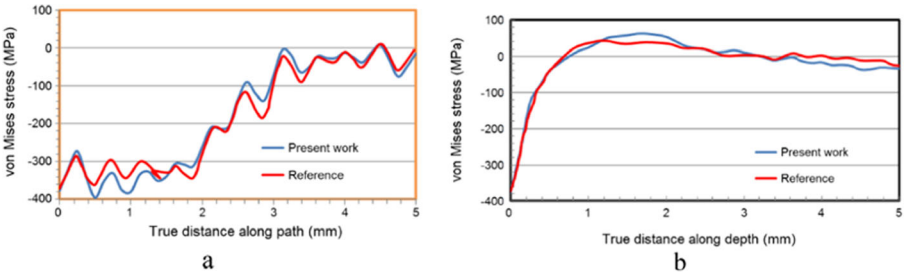

Fig. 9 Comparison between present work and reference [32]. S33 after 4000 ns (**a**) Along Z direction. (**b**) Along depth

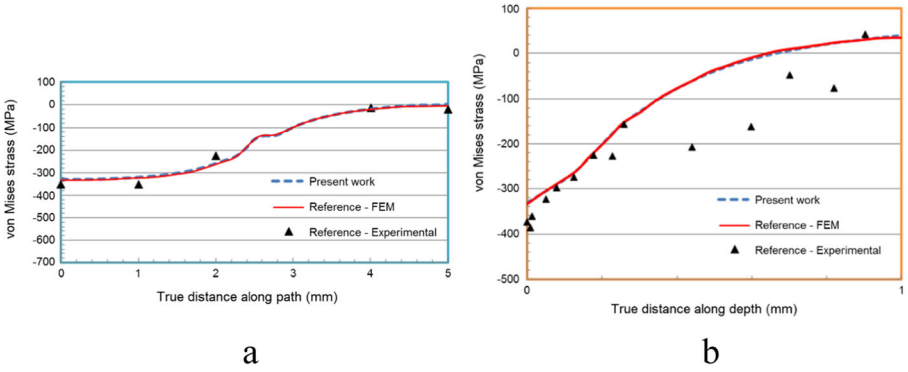

Fig. 10 Comparison between present work and references [32, 37] for S33 RS (**a**) Along Z direction. **b** Along depth

convergence test for determining the suitable mesh size was performed. In order to select the most suitable mesh size, it was investigated along two directions, i.e., the surface, and the depth (Fig. 13) of model. The model was simulated with different mesh sizes and the mean of dynamic von Mises stress was derived along specified paths (Fig. 14). Obviously when the mesh size is converged for dynamic stresses, it will be acceptable for residual stresses either, hence, mesh convergence is done for dynamic analysis only.

Based on the results shown in Fig. 14 and considering the importance of mesh size discussed before, the maximum reliable mesh sizes on the surface and in depth were decided to be 0.2 mm and 0.15 mm respectively. For further reduction of computational time and cost, and considering approximate 1 mm penetration depth of residual stresses, mesh size of 0.15 mm was considered up to the depth of 2 mm, and then increased to 0.25 mm.

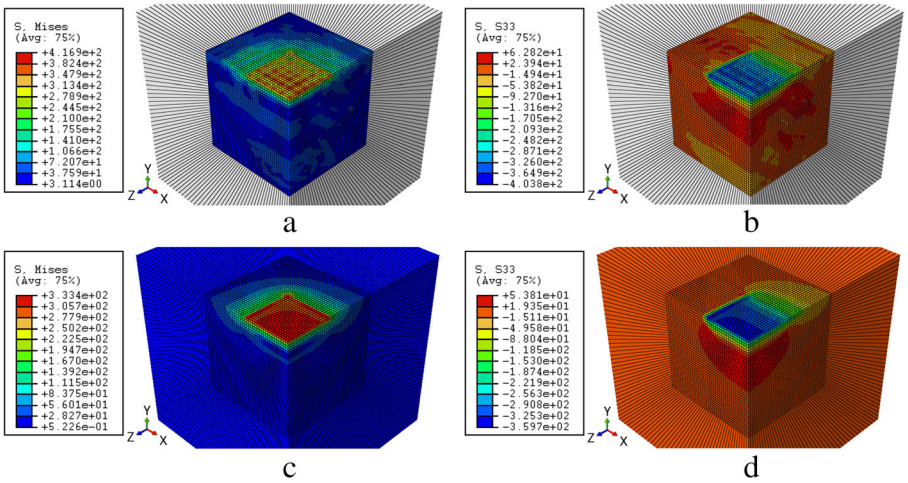

Fig. 11 Stress distribution (**a**) von Mises after 4000 ns. (**b**) S33 after 4000 ns. (**c**) von Mises residual stress. (**d**) S33 residual stress

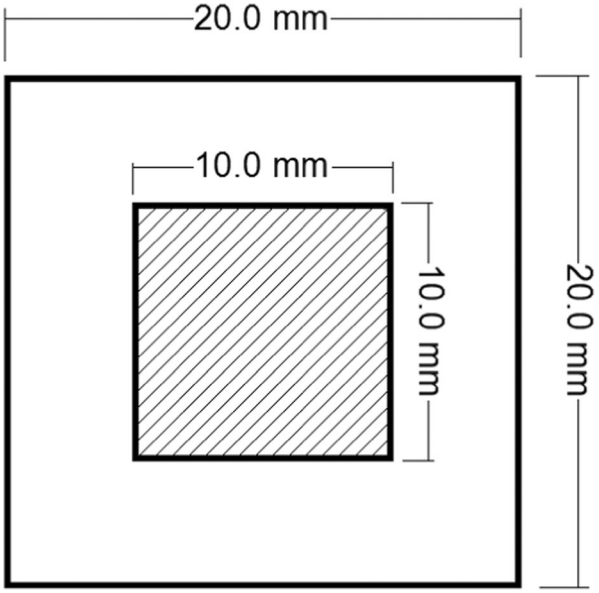

Fig. 12 Specimen geometry

After completing both static and dynamic analyzes, the distribution of RSs on the surface and in the depth of the sample was determined. Figure 15-a and b illustrate the distribution of von-Mises and tangential RS on the sample surface respectively. The maximum absolute values of tangential compressive residual stresses, shown with dark blue color, were about 1000 MPa and located on the overlapping region of two laser pulses. Nonetheless, the least value of compressive residual stresses, shown with green color, was found to be 400 MPa and located in the areas between the laser pulses. Therefore, in order to acquire a uniform distribution of the residual compressive stresses, the optimum distance between laser pulses should be determined.

Optimization

The first step in any optimization process is to specify the optimization variables, constraints and objective function(s). The optimization variables in this study are those

Table 2 Mechanical properties of Inconel 718 [36]

Mechanical property	Value
Mass density (g/cm3)	8.11
Young's modulus at 20 °C (GPa)	201
Yield stress (MPa)	950
Ultimate tensile stress (MPa)	1095

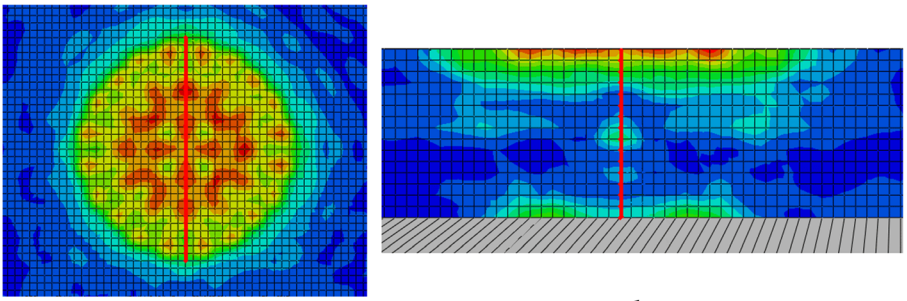

Fig. 13 Measurement paths (**a**) On the surface (**b**) In depth

parameters that directly affect the RSs in LSP process. These parameters along with their types and allowable ranges or choices, are discussed in Table 3.

In order to compare and investigate the effect of laser beam shape and contact area, different sizes of circular, ovals with three different diameter ratios, and square shapes were simulated. It must also be noted that in triangular scan algorithm, the starting point in every even rows moved half of the shooting pitch forward along X direction. Variation of X and Y pitch affected the percentage of overlapping of every two consecutive laser beams, so they could be overlapped, tangent, or with a gap. However, in order to maintain the symmetry of the model, equal X and Y pitches were considered for circular and square shapes, while for oval laser beams, the ratio of X and Y pitch was assumed to be equal to the oval large to small diameter ratio. Hence, if there was a percentage of overlap or gap, this value would be the same in two directions. Equation 5 shows the concept of calculating shooting pitch (P), for oval laser shapes, in which D and d are the large and small oval diameters respectively.

$$\begin{aligned} P_x &= P \\ P_y &= \left({}^{D}/_{d}\right)P \end{aligned} \tag{6}$$

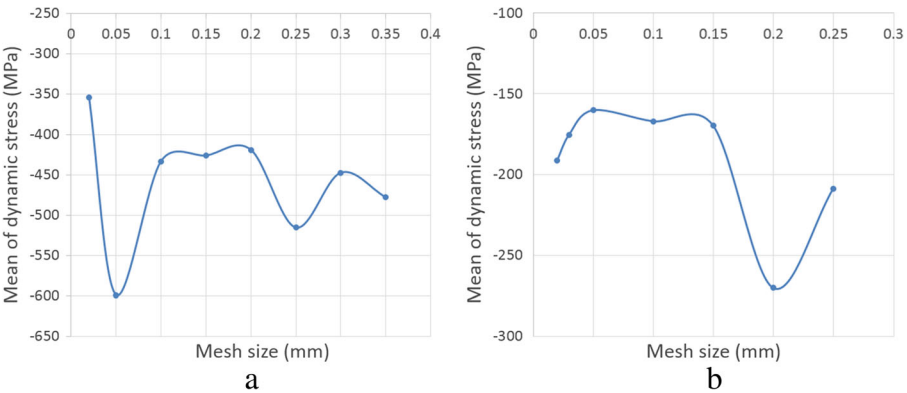

Fig. 14 Mean RS for different mesh sizes (**a**) On the surface. (**b**) In depth

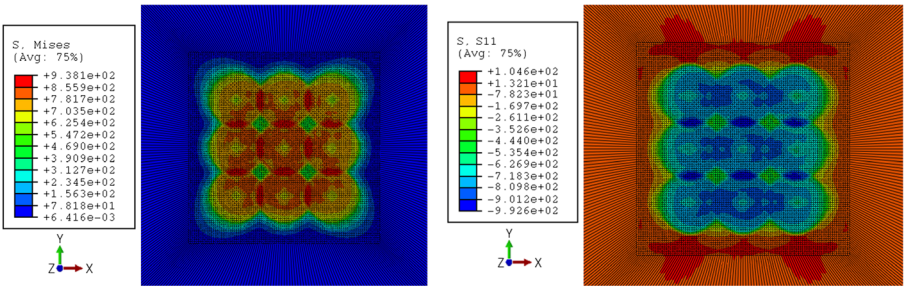

Fig. 15 RS distribution on surface (**a**) Von Mises (**b**) S11

The next step in optimization process was to specify the optimization constraints. These constraints were specified according to the main objective of this research, which was to generate a relatively uniform compressive RS up to a specified depth of a part. Consequently, the following constraints were defined:

- The maximum absolute value of compressive RS should be more than 500 MPa.
- The penetration depth of RS should be greater than 1 mm.

It should be noted that penetration depth includes the area in which the compressive RS is more than 20Mpa.

The next step of optimization was to determine objective function(s). The proposed objective functions were: minimizing the percentage of RS non-uniformity, and minimizing the financial cost of LSP process. Obviously increasing

Table 3 Optimization variables and ranges

Parameter	Type	Range
Laser power (GW)	Continuous	0.1 ~ 10
Laser beam radius (mm)	Discrete	1 ~ 5 with 0.2 mm steps
Scan pitch (mm)	Discrete	2 ~ 10 with 0.2 mm steps
Scan pattern	Discrete	Square / Triangular
Laser beam shape	Discrete	Square (Sideways equal to radius) 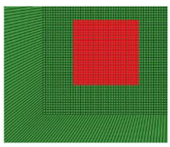
		Oval with large to small diameter ratios of 1 (circular), 0.75, 0.5 and 0.25 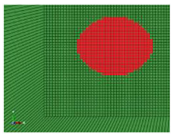

the number of shoots and LSP energy would ensure the achievement of the constraints, however, this will surely lead to application of more powerful laser machine and consequently increasing the cost of LSP process. Since two objectives should be considered together in this analysis, one of multi objective optimization problems should be employed for determining the optimum LSP parameters. In this study, weight function method was implemented, in which, after determining each objective function, F_i; the general coefficients or weights of the functions, W_i, were specified and linearly combined to form the multi-objective function, U; according to Eq. 7 [38]:

$$U = -\sum_{i=1}^{k} \mathrm{W}_i \mathrm{F}_i \tag{7}$$

Here, the first objective function was the percentage of non-uniformity (ΔR), which was determined for the elements on the surface of part as follows:

$$\Delta \mathrm{R} = \frac{|\mathrm{S}_{\max} - \mathrm{S}_{\min}|}{|\mathrm{S}_{\max}|} \tag{8}$$

In Eq. 8, ΔR is the percentage of non-uniformity of compressive RS on the surface, and S_{max} and S_{min} are the highest and the lowest resulted compressive RSs respectively.

The second function was the cost of performing LSP process (C). Since for LSP process adequate amount of peening and its parameters must be clarified and try to avoid over-peening the surface, it was found that the best solution that covers all these intentions is cost function. Increasing energy or using larger laser machine, over-peening, improper peening pitch, etc. will all affect the cost of LSP process. Therefore, it was decided to choose the cost as the most suitable objective during this research. A referenced case study beside market information was used during this research to specify a linear cost function in this research. This function can be defined by a linear function of pulses number and laser energy, whose coefficients can be attained from industry and laser machining market (Eq. 9):

$$Cost = aNj + b\ (\$) \tag{9}$$

Where N and J represent the number of pulses and employed laser energy (Joule) respectively. To obtain the values of a and b coefficients in the cost function, information acquired from various laser research centers was used in here. Noting that this data, obviously, can vary depending on industrial and economic conditions. Based on this information, 1000 pulses of laser with 200mj and 500mj of power cost 30$ and 60$ respectively. Accordingly, the mentioned coefficients were calculated, and the cost function was assumed as Eq. 10:

$$Cost = 0.1Nj + 10\,(\$) \tag{10}$$

The next step after obtaining objective functions was to determine their weights. Not only these coefficients should include the weight and importance of each function, but also, they should balance their order. Accordingly, as illustrated in Table 4 the results of two different simulations were used to roughly estimate these coefficients. However, some optimization constraints, like minimum depth or minimum amount of RS, could not easily be met in the experiments mentioned in Table 4. To satisfy these constraints more energy and lower peening pitch are required to fulfill the constraints which leads to additional cost presented for the 2nd experiment, while the difference between the amounts of non-uniformity between 2 experiments does not look much. The information mentioned in Table 4 were also used to acquire weights of Cost and Non-uniformity function.

Since the order of cost function was much larger than the order of non-uniformity percentage function, coefficient υ was defined for non-uniformity function to balance the order of these two functions. Thus the balanced optimization function was defined as in Eq. 11.

$$F = C + \upsilon \Delta R \tag{11}$$

Using the values listed in Table 4, the final multi objective function was obtained as follows [39]:

$$F = C + 5783 \Delta R \tag{12}$$

Obviously considering variable weights for the functions, would lead to generation of Pareto frontier which includes all combinations of weight ratios for the objective functions, and can be investigated in further researches. Finally by Eq. 12, the multi-objective optimization problem is now converted to a single-objective optimization, and can be solved by any heuristic method.

Particle Swarm Optimization (PSO) is a population based evolutionary algorithm, which is inspired from the nature and employs population intelligence to find the optimum states. Here, this method which has reasonable calculation time and acceptable convergence speed, was utilized in ABAQUS PDE environment. In this algorithm, an initial amount from the variables feasible region was randomly assigned to particles position vectors: $X = [x_1, x_2, \ldots, x_j]$. Using FE analysis, every particle was used to determine the value of fitness (objective) function $f[X_1^{(0)}]$, $f[X_2^{(0)}]$ …, $f[X_N^{(0)}]$ while considering the constraints. By calculating the movement speed, and by special consideration of the best recorded experiences of the objective function encountered in all previous iteration ($P_{g.Best}$) and the highest value of objective function in the previous iteration ($P_{i.\,Best}$), these particles then move toward new locations in the design

Table 4 Peening process costs and non-uniformities for 2 experiments

Experiment No.	Cost ($)	Non-uniformity %
1	318	29
2	665	23

hyperspace. The velocity V and position X of each particle in the design hyperspace, and updating mechanism were shown by Eq. 13 [39].

$$\begin{aligned} &X_i = (x_{i_1}, x_{i_2}, x_{i_3}, \ldots, x_{i_6}) \\ &V_i = (v_{i_1}, v_{i_2}, v_{i_3}, \ldots, v_{i_6}) \\ &V_i(t) = w \times V_i\,(t{-}1) + C_1 \times rand_1 \times (P_{i.best}{-}X_i\,(t{-}1)) + C_2 \times rand_2 \times \\ &(P_{g.best}{-}X_i\,(t{-}1))X_i = X_i\,(t{-}1) + V_i(t) i = 1, 2, 3, \ldots, N \end{aligned} \tag{13}$$

C_1 and C_2 are individual and social learning rates respectively, r_1 and r_2 are random numbers between 0 and 1. Moreover, θ is the inertia weight used to balance between global and local exploration, which speeds convergence up to true optimum (Eq. 14) [39]:

$$\theta\,(i) = \theta_{max} - \left(\frac{\theta_{max} - \theta_{min}}{i_{max}}\right) \times i \tag{14}$$

θ_{max} and θ_{min}, normally set to 0.9 and 0.4 respectively, are the initial and final values of the inertia weight. It is also noted that when the constraint, $g_j\,(X) \le 0$, $i = 1, 2, \ldots, m$ are present in optimization problem, penalty functions are added to the objective function(s). (Eq. 15)

$$F\,(X) = f\,(X) + C\,(i)\,H\,(X) \tag{15}$$

Where $C(i)$ and $H(X)$ denote a dynamically modified penalty parameter that varies with the iteration number i and penalty factor associated with the constraints respectively, as shown in Eq. 16 [39]:

$$\begin{aligned} &C\,(i) = (ci)^{\alpha} \\ &H\,(X) = \sum_{j=1}^{m} \left\{ \varphi\left[q_j(X)\right] \left[q_j\,(X)\right]^{\gamma[q_i\,(X)]} \right\} \\ &\varphi\left[q_j\,(X)\right] = a\left(1 - \frac{1}{e^{q_j\,(X)}}\right) + b \\ &q_j\,(X) = \max\left\{0, g_j(X)\right\}, \\ &j = 1, 2, 3, \ldots, m \end{aligned} \tag{16}$$

The values of a, b, c, and α are equal to 150, 10, 0.5, and 2 respectively, along with $\gamma\,[q_j\,(X)]$ which is addressed in Eq. 17 [39]:

$$\gamma\left[q_j\,(X)\right] = \begin{cases} 1 & q_j\,(X) \le 1 \\ 2 & q_j\,(X) > 1 \end{cases} \tag{17}$$

In this coupled FE-PSO problem, a new population from the domains defined in Table 3 was randomly generated. After simulating laser peening with the proposed variables for each particle, generated RSs together with LSP costs were determined, and their amount and penetration depth in part were checked. If the constraints were satisfied

the next population would be created, otherwise, the objective function as modified by Eqs. 16 and 17, would be determined and the iteration would continue with the next steps of search and updated population. The new positions of particles were then generated using PSO method and once again these steps were continued till the number of iterations reaches the specified value or the results converges (Fig. 16). Depending on the amounts of coefficients C_1 and C_2 in Eq. 12, the convergence speed and number of iterations has been varied.

To solve this FE-PSO problem, it was decided to use PDE environment inside ABAQUS software and coding based on Python programming language. In comparison with linking FE software and a mathematical software, e.g. MATLAB, this method enormously decreased calculation time and made the study more flexible. Thus, the optimization process was performed in ABAQUS FE software to prevent frequent data transfer between two software. Firstly, the FE model was parametrically designed to be able to take input values automatically. Then 100 particles were defined in the feasible region and random values were generated out of their domains to make design vectors, which were then automatically included in the simulation program variables. Thus, a new model was generated for each particle and analyzed by ABAQUS software. The maximum and minimum compressive RSs on the surface as well as penetration depth of compressive RSs were extracted from the results, and an error function in the objective function was included in case the constraints were not met. Afterward, the objective function for particles were renewed, and the PSO algorithm generated the next values for the particles. By continuing these steps and after a number of iteration the optimum results were revealed. Due to the enormous amount of calculation and simulation steps, only 30 iterations took about 70 days for a Corei7 desktop computer to perform this calculation, therefore for completing the optimization process a super computer with 5 nodes each having 48 computing cores and 100GB of RAM was employed.

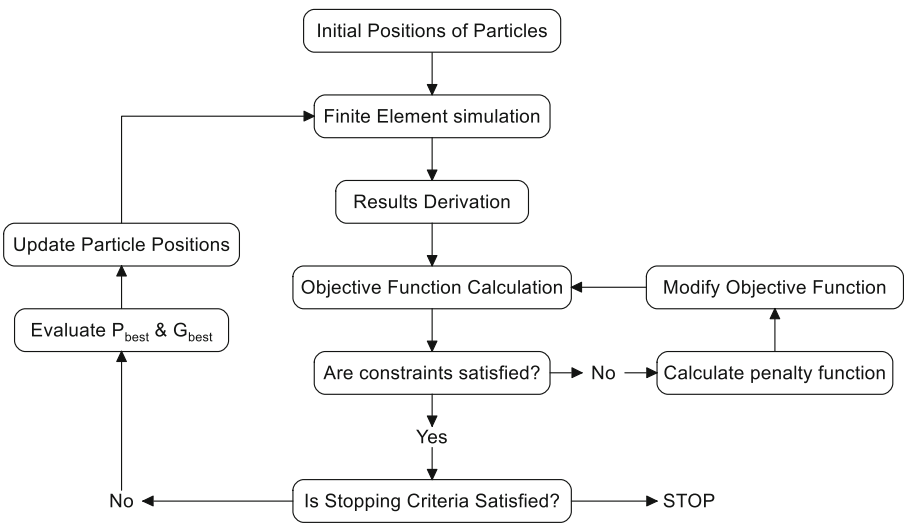

Fig.16 Optimization flowchart

The optimum parameters determined during this research were the best input values for the process and led to the highest uniformity of RS on the surface with minimum cost as follows:

- Laser beam radius: 2.8 mm
- Laser power: 2.1 GW
- Step: 3.4 mm
- The shape of the laser effect point: Circular
- Surface Scanning pattern: Square

By applying these values to the process, the following results were obtained:

- Maximum compressive residual stress: -735 MPa
- Minimum compressive residual stress: -478 MPa
- Non-uniformity percentage: 35%
- Residual stress depth: 1.05 mm
- The value of the cost function: 329
- The value of the target function: 2353

Von Misses and S11 RS distribution on the surface and depth of the model simulated by optimum parameters were shown in Fig. 17. It should be noted that some RSs resulted by supports' reactional forces could be seen in the specimen which are far enough from treated surface to not interfere with LSP RSs.

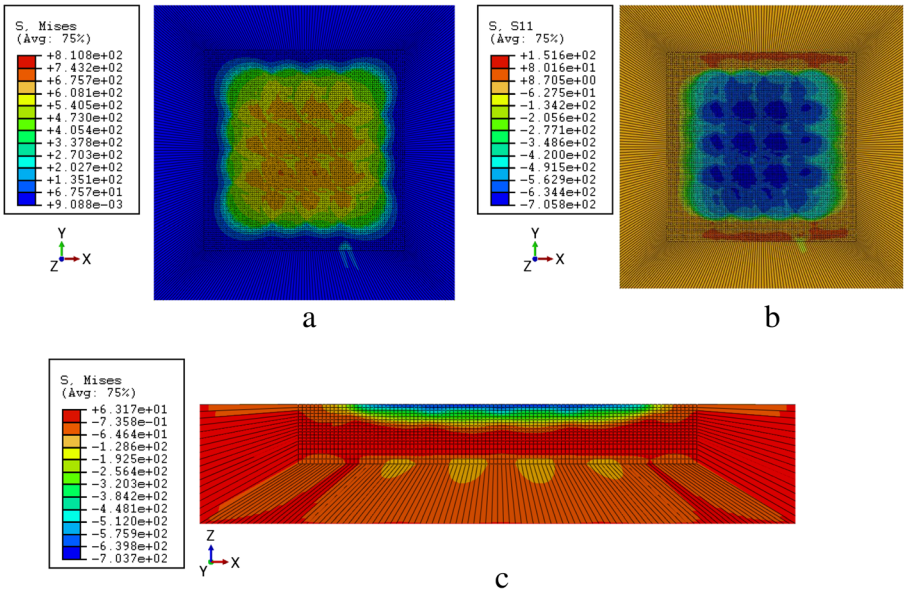

Fig. 17 RS distribution using optimum parameters. (**a**) Von Mises on surface. (**b**) S11 on surface. (**c**) S11 in depth

To validate the effectiveness of the optimization process one solution is to simulate the model using a new set of parameters with a small or large deviation from the optimum ones. To show the effect of changing beam shape on the results, all optimum variables listed above were kept unchanged except the laser beam shape, which was changed from circle to square. The simulation depicted that the minimum and maximum generated RSs were -681 MPa and -417 MPa respectively which leads to 39% non-uniformity, and also maximum depth of 0.9 mm, so that both were worse than the optimum results as shown in Fig. 18. Furthermore, other experiments with more deviation from the optimum variables were considered and simulated, and none of them leaded to better objectives proposed in this research.

Discussion and Conclusion

A finite element simulation and optimization method for determining the optimum parameters for laser shock peening process was obtained and presented to optimize the process mechanically and financially. Laser power, beam diameter, peening pitch, beam shape, and peening pattern were the most affecting parameters on the quality of LSP process determined in this study. Two constraints beside two objective functions were

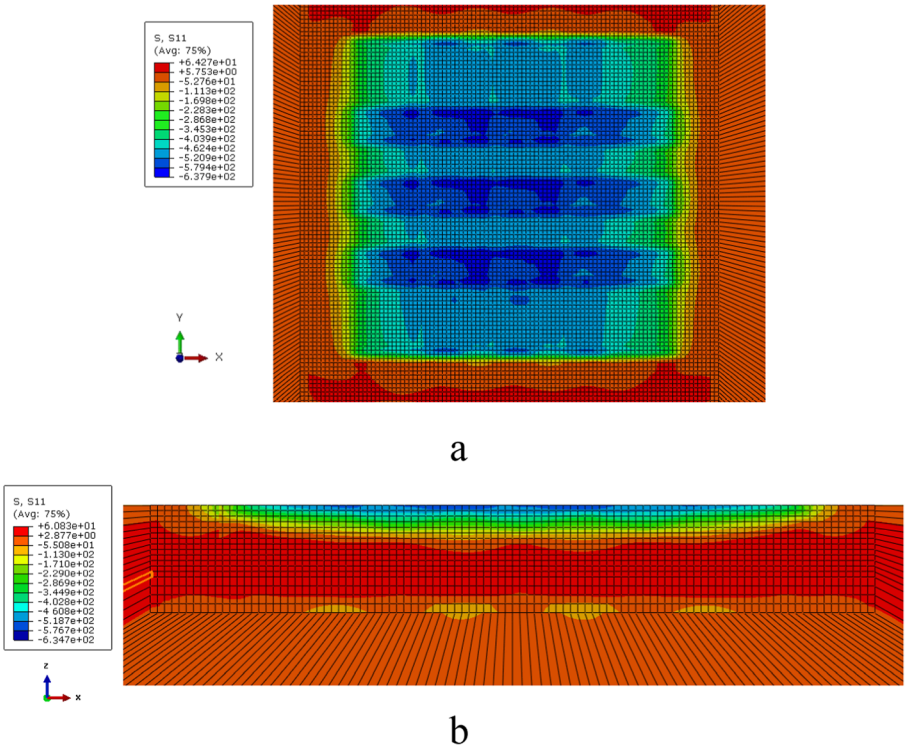

Fig. 18 Distribution of RS on (**a**) surface and (**b**) depth of the model using square shape beam

proposed for optimization. Minimum required amount of RS and effective depth were considered as constraints, and non-uniformity of RS distribution along with cost of LSP were considered as the objective functions for optimization.

It was found that, reducing the peening pitch, while satisfying the constraints, would improve the non-uniformity, but will increase the peening cost. The same discussion is true when increasing the laser beam diameter or laser power. Since this multi-objective optimization process was changed to a single objective one by certain weights for the objectives, changing the weight of functions will surely lead to different optimum variables, that any researcher may set the weights according to their needs and priorities.

Finally, the obtained results are summarized as follows:

- A complete methodology for simulating laser shock peening process was presented and this methodology can be used for any other LSP simulation process.
- PSO algorithm was proposed to determine the optimum laser peening parameters considering minimum amount of RS and the penetration depth as constraints, and non-uniformity of the RSs and cost of LSP as objective functions.
- In order to have a straightforward methodology, more accuracy in optimization, and avoid dependency on different types of software, optimization process and finite element simulation were coupled together in the ABAQUS PDE environment.
- It was found that the RSs are more uniform at lower laser powers, however it may not satisfy the constraints.
- Reducing the radius of laser beam directly increases both non-uniformity of RSs and cost of peening operation.
- Size and shape of the laser beam were considered for the first time as optimization variables, and it was shown despite the fact that square shape seems to have better affect, the most suitable laser beam cross section is circle, which is applied by square scanning pattern. Moreover, the optimal laser beam radius was found to be 2.8 mm for the proposed material and weights for the objectives.
- The highest uniformity was considered as an optimization goal for the first time, and simultaneous consideration of cost function as another objective led to minimum non-uniformity of 35%.
- The optimal amount of overlap percentage of beams was found to be 32% in this case.
- The minimum cost of laser shock peening process with the least percentage of RSs non-uniformity on the surface, was found to be $329, which may vary by updating the price list and changing the cost weight in objective function.
- Considering higher cost of the process in optimal conditions in comparison with 2 presented experiences before (Table 4), it can be concluded that, despite generation of proper amount of RS on the treated surface, more effort is needed for the RSs to penetrate into acceptable depth of the part, which reminds the necessity of optimization for this process.

Acknowledgements The authors wish to thank the University of Kashan for supporting this research by grant No. 682570.

References

1. Thompson, S.D., See, D., Lykins, C., Sampson, P.: Laser shock peening vs. shot peening–a damage tolerance investigation. In: Minerals, Metals and Materials Society (TMS) /AIME(USA), vol. **48**, pp. 239–251 (1996)
2. Irizalp, S.G., Saklakoglu, N., Akman, E., Demir, A.: Pulsed Nd: YAG laser shock processing effects on mechanical properties of 6061-T6 alloy. Opt Laser Technol. **56**, 273–277 (2014)
3. Kattoura, M., Mannava, S.R., Qian, D., Vasudevan, V.K.: Effect of laser shock peening on residual stress, microstructure and fatigue behavior of ATI 718Plus alloy. Int J Fatigue. **102**, 121–134 (2017)
4. Hassan, S.S., Hamzah, M.N., Abed, R.M.: The effect of laser shock peening on fatigue life using pure water and hydrofluoric acid as a confining layer of Al–alloy 7075-T6. J Eng. **24**(1), 207–217 (2018)
5. Mannava, S., Ferrigno, S.J.: Laser shock peening for gas turbine engine vane repair. In. Google Patents, US5584662A (1997)
6. Ferrigno, S.J., McAllister, K.G., Mannava, S.: Laser shock peened gas turbine engine seal teeth. In. Google Patents, US6200689B1 (2001)
7. Fabbro, R., Fournier, J., Ballard, P., Devaux, D., Virmont, J.: Physical study of laser produced plasma in confined geometry. J Appl Phys. **68**(2), 775–784 (1990)
8. Wu, B., Shin, Y.C.: A self-closed thermal model for laser shock peening under the water confinement regime configuration and comparisons to experiments. J Appl Phys. **97**(11), 113517–1-11), (2005)
9. Wu, B., Shin, Y.C.: A one-dimensional hydrodynamic model for pressures induced near the coating-water interface during laser shock peening. J Appl Phys. **101**(2), 023510–1-5), (2007)
10. Wu, B., Shin, Y.C.: Two dimensional hydrodynamic simulation of high pressures induced by high power nanosecond laser-matter interactions under water. J Appl Phys. **101**(10), 103514–1-8), (2007)
11. Wu, B., Shin, Y.C.: From incident laser pulse to residual stress: a complete and self-closed model for laser shock peening. J Manuf Sci Eng. **129**(1), 117–125 (2007)
12. Cao, Y., Shin, Y.C., Wu, B.: A parametric study on overlapping laser shock peening of 4140 steel via modeling and experiments. ASME International Manufacturing Science and Engineering. **132**(6), 245–254 (2008)
13. Wei, X., Ling, X.: Numerical modeling of residual stress induced by laser shock processing. Appl Surf Sci. **301**, 557–563 (2014)
14. Keller, S., Chupakhin, S., Staron, P., Maawad, E., Kashaev, N., Klusemann, B.: Experimental and numerical investigation of residual stresses in laser shock peened AA2198. J Mater Process Technol. **255**, 294–307 (2017)
15. Kim, J.-S., Nam, H.-S., Kim, Y.-J., Kim, J.-H.: Numerical Study of Laser Shock Peening Effects on Alloy 600 Nozzles With Initial Residual Stresses. J Press Vessel Technol. **139**(4), 041406 139–147), (2017)
16. Warren, A., Guo, Y., Chen, S.: Massive parallel laser shock peening: simulation, analysis, and validation. Int J Fatigue. **30**(1), 188–197 (2008)
17. Huang, S., Zhu, Y., Guo, W., Peng, P., Diao, X.: Impact toughness and microstructural response of Ti-17 titanium alloy subjected to laser shock peening. Surf Coat Technol. **327**, 32–41 (2017)
18. Wu, B., Tao, S., Lei, S.: Numerical modeling of laser shock peening with femtosecond laser pulses and comparisons to experiments. Appl Surf Sci. **256**(13), 4376–4382 (2010)
19. Xu, G., Luo, K., Dai, F., Lu, J.: Effects of scanning path and overlapping rate on residual stress of 316L stainless steel blade subjected to massive laser shock peening treatment with square spots. Appl Surf Sci. **481**, 1053–1063 (2019)
20. Sathyajith, S., Kalainathan, S.: Effect of laser shot peening on precipitation hardened aluminum alloy 6061-T6 using low energy laser. Opt Lasers Eng. **50**(3), 345–348 (2012)
21. Prabhakaran, S., Kulkarni, A., Vasanth, G., Kalainathan, S., Shukla, P., Vasudevan, V.K.: Laser shock peening without coating induced residual stress distribution, wettability characteristics and enhanced pitting corrosion resistance of austenitic stainless steel. Appl Surf Sci. **428**, 17–30 (2018)
22. Singh, G.: Effective Simulation and Optimization of a Laser Peening Process. Wright State University, Dr. Thesis (2009)
23. Chupakhin, S., Klusemann, B., Huber, N., Kashaev, N.: Application of design of experiments for laser shock peening process optimization. Int J Adv Manuf Technol. **102**(5–8), 1567–1581 (2019)
24. Sibalija, T.V., Petronic, S.Z., Majstorovic, V.D., Milosavljevic, A.: Modelling and optimisation of laser shock peening using an integrated simulated annealing-based method. Int J Adv Manuf Technol. **73**(5–8), 1141–1158 (2014)

25. Amarchinta, H.K., Grandhi, R.V., Clauer, A.H., Langer, K., Stargel, D.S.: Simulation of residual stress induced by a laser peening process through inverse optimization of material models. J Mater Process Technol. **210**(14), 1997–2006 (2010)
26. Zhao, J., Dong, Y., Ye, C.: Laser shock peening induced residual stresses and the effect on crack propagation behavior. Int J Fatigue. **100**, 407–417 (2017)
27. Frija, M., Ayeb, M., Seddik, R., Fathallah, R., Sidhom, H.: Optimization of peened-surface laser shock conditions by method of finite element and technique of design of experiments. Int J Adv Manuf Technol. **97**(1–4), 1–19 (2018)
28. Ayeb, M., Frija, M., Fathallah, R.: Prediction of residual stress profile and optimization of surface conditions induced by laser shock peening process using artificial neural networks. Int J Adv Manuf Technol. **100**(9–12), 2455–2471 (2019)
29. Bhamare, S., Ramakrishnan, G., Mannava, S.R., Langer, K., Vasudevan, V.K., Qian, D.: Simulation-based optimization of laser shock peening process for improved bending fatigue life of Ti–6Al–2Sn–4Zr–2Mo alloy. Surf Coat Technol. **232**, 464–474 (2013)
30. Kumar, G.R., Rajyalakshmi, G.: Modelling and multi objective optimization of laser peening process using Taguchi utility concept. In: IOP Conference Series: Materials Science and Engineering 2017, **263**(6), p. 062055. IOP Publishing
31. Masse, J.-E., Barreau, G.: Surface modification by laser induced shock waves. Surf Eng. **11**(2), 131–132 (1995)
32. Ding, K., Ye, L.: Laser shock peening: performance and process simulation. In: Ding, K., Ye, L. (eds.) Simulation methodology, pp. 47–72. Woodhead Publishing, Abington, Cambridge (2006)
33. Peyre, P., Scherpereel, X., Berthe, L., Fabbro, R.: Current trends in laser shock processing. Surf Eng. **14**(5), 377–380 (1998)
34. Peyre, P., Fabbro, R., Merrien, P., Lieurade, H.: Laser shock processing of aluminium alloys. Application to high cycle fatigue behaviour Materials Science and Engineering: A. **210**(1–2), 102–113 (1996)
35. Devaux, D., Fabbro, R., Tollier, L., Bartnicki, E.: Generation of shock waves by laser-induced plasma in confined geometry. J Appl Phys. **74**(4), 2268–2273 (1993)
36. Braisted, W., Brockman, R.: Finite element simulation of laser shock peening. Int J Fatigue. **21**(7), 719–724 (1999)
37. Ballard, P., Fournier, J., Fabbro, R., Frelat, J.: Residual stresses induced by laser-shocks. Phys. IV France. **01**(C3), C3–487-C483–494), (1991)
38. Marler, R.T., Arora, J.S.: Survey of multi-objective optimization methods for engineering. Struct Multidiscip Optim. **26**(6), 369–395 (2004)
39. Trelea, I.C.: The particle swarm optimization algorithm: convergence analysis and parameter selection. Inf Process Lett. **85**(6), 317–325 (2003)